Low Temperature Physics/Fizika Nizkikh Temperatur, 2012, v. 38, No. 8, pp. 923–931

Orientational glassification in fullerite C_{60} saturated with H_2: photoluminescence studies

P.V. Zinoviev, V.N. Zoryansky, N.B. Silaeva, Yu.E. Stetsenko, M.A. Strzhemechny, and K.A. Yagotintsev

B. Verkin Institute for Low Temperature Physics and Engineering of the National Academy of Sciences of Ukraine
47 Lenin Ave., Kharkov 61103, Ukraine
E-mail: strzhemechny@ilt.kharkov.ua

Received March 20, 2012

Using one-photon excitation we studied photoluminescence of C_{60} saturated with molecular hydrogen over a temperature range 10 to 230 K. Saturation of samples was done at a pressure of 30 atm and at temperatures low enough (T < 250 °C) to exclude chemical sorption. The samples were saturated during periods of varied duration τ to reach different occupancy levels. To check reliability of our luminescence results and interpretation, our spectra for pure C_{60} were compared with data known in the art, demonstrating good compatibility. The luminescence spectra were attributed according to the approach of Akimoto and Kan'no by separating total spectra in two components of different origin. The A-type spectra, which are associated with exciton transport to deep traps, above 70 K become prevail over the B-type emission. Until saturation times did not exceed a certain value (for one, 50 h for a saturation temperature of 200 °C) the integrated intensity I as a function of the temperature T of luminescence measurements, $I(T)$, remained at a constant level up to the orientational vitrification point of about 100 K and then went rather steeply down with increasing T. However, at longer τ the intensity $I(T)$ persisted in constancy to higher T (the higher, the longer τ) and then dropped with increasing T. This finding made us to reexamine more closely the lattice parameter vs saturation time dependence for saturation temperatures 200 and 230 °C. As a result, additional evidence allowed us to infer that after completion of the single-molecule filling of O-voids (specifically, after roughly 50 h for T_{sat} = 200 °C) a slower process of double filling sets in. Double filling entails an anisotropic deformation of the octahedral cage, which modifies rotational dynamics stronger than single filling. Further, we argue that singlet exciton transport to traps (which is responsible for the A-type emission) can be crucially hampered by rotational jumps of one of the molecules over which a travelling exciton is spread. Such jumps break coherence and the exciton stops thereby increasing the probability of emissionless deactivation. If so, then the temperature, at which the rotational jumps occur sufficiently frequently, may be by inference considered the unfreezing point for the orientational glass state (essentially coinciding with the inverse critical point T_g where the rotational system freezes into the orientational glass). This treatment of T_g differs from that existing in the art according to which the glass state is destroyed owing to the increased density of phonon states. Keeping to our reasoning, we conclude that the orientational glass state does not disappear but, instead, is conserved almost unchanged under one-molecule feeling and persists to appreciably higher temperatures in the case of double filling, which affects exciton dynamics stronger.

PACS: *81.05.ub* Fullerenes and related materials;
78.55.–m Photoluminescence, properties and materials;
61.43.–j Disordered solids;
78.55.Qr Amorphous materials; glasses and other disordered solids.

Keywords: pure and H_2-doped fullerite C_{60}, photoluminescence, orientational glassification, exciton transport.

1. Introduction

Fullerite C_{60} belongs to the class of molecular crystals in which molecules are mutually bound by a relatively weak van der Waals forces. Unlike in other classical molecular crystals, in which the molecules sit tight in the crystal lattice, fullerite C_{60}, in which molecules can rotate, resembles such cryocrystals as nitrogen or methane. Charge transport [1,2] and other physical properties of C_{60} depend on the orientational ordering of molecules and the presence

of interstitial impurities in the crystal lattice. At room temperature, fullerite has a face centered cubic lattice, in which the molecules rotate almost freely [3,4]. In this structure there is one large interstitial void (of radius 2.1 Å) of octahedral (O) symmetry and two smaller voids (of radius 1.1 Å) of tetrahedral (T) symmetry per each fullerene molecule [5]. Those voids are large enough to reversibly accommodate rare gas atoms and compact molecules [6–13]. These intercalants influence the state of orientational order of fullerene molecules in the crystal lattice. In particular, in doped C_{60} the temperatures related with orientational ordering and orientational vitrification shift and hysteretic phenomena are be observed in these critical regions. When C_{60} crystals are intercalated with CO and NO molecule [14–17] to high occupancies of octahedral voids, the specific singularities around the glassification transition disappear. These findings were treated as the proof of an essential saturation-related increase in the concentration of mutual pentagon orientations of molecular pairs and, thereby, put to suspicion the very existence of the orientational glass state in concentrated interstitial solid mixtures of CO and NO with C_{60}. It should be noted that the role of chemically neutral interstitial impurities in the modification of rotational states of C_{60} is not completely understood. For example, arguments exist that such impurities facilitate *polyamorphic* first-order transformations between different states of the orientational glass [18,19]. The above considerations and conclusions should be checked using an independent experimental method. This article is an attempt to accomplish that using the photoluminescence method, which proved its efficiency in studies of fullerite C_{60} saturated with chemically neutral particles [20,21].

Presence of an impurity particle in the crystal lattice of C_{60} noticeably affects its optical properties. The photoluminescence spectrum of fullerite C_{60} is determined by various emitting entities such as Frenkel excitons [22,23], charge-transfer excitons [24], and the so-called deep X-traps [22,23,25,26], most likely, associated with structure defects and impurities. Using luminescence data it has been demonstrated [20] that emission from X-traps and the variation of the integrated photoluminescence intensity can be a powerful instrument in studying effects of intercalation on the orientational ordering of fullerene molecules in the C_{60} crystal lattice.

In this article we studied over the temperature range 10–230 K the photoluminescence of small C_{60} single crystals doped with molecular hydrogen. Our main aim was to elucidate how impurity hydrogen molecules influence the formation of the orientational glass state of C_{60}. The choice of C_{60} single crystals stuffed with H_2 impurities as the object of study was not occasional. Hydrogen molecules with a van der Waals radius of 1.2 Å can be accommodated in O-cavities in pairs [27,28]. In addition, hydrogen was chosen as the most suitable dopant from other considerations. In spite of the fact that the saturation process with He as dopant has been studied [11] in more detail, utilization of helium as dopant turned out to be impractical since we were unable to saturate C_{60} with He *in situ* when carrying out optical measurements, whereas transplanting a sample from the saturator to the optical camera was accompanied by a noncontrollable degassing, especially from subsurface layers. It should be also added that in experiments involving a He–Ne laser (E_{exc} = = 1.96 eV) the penetration depth for exciting photons is of order of a few microns [29]. On the other hand, a hydrogen molecule interacts with carbon atoms much stronger that a helium atom and one could expect the effect of H_2 on the rotational state of C_{60} to be sufficient for documenting the consequences.

For a more reliable interpretation of photoluminescence data, the process of saturation of C_{60} with hydrogen was controlled and monitored using powder x-ray diffraction. The relevant results of those x-ray studies, of importance in themselves, are published independently [30].

In conclusion we also add that details of the interaction of hydrogen with fullerite C_{60} is part of a wider circle of investigations in the development of notions and ideas pertaining to the interaction of hydrogen with other novel nanostructured carbon materials (including nanotubes and graphene) which can be utilized for accumulation, storage and transport of hydrogen.

2. Experimental technique and samples

The typical dimensions of C_{60} single crystals for these studies were $0.5\times0.5\times0.5$ mm. A detailed description of the process of stuffing C_{60} single crystals with hydrogen as well as the relevant characterization of samples can be found elsewhere [30]. Luminescence studies of C_{60} intercalated with molecular hydrogen were carried out with a setup which allowed us to register emission from sources with low quantum output over a wide temperature range (10–300 K). Luminescence emission of C_{60} was stored in the reflection regime within a spectral range of 1.2–1.85 eV ($1033-670$ nm) with the aid of a MDR-2 diffraction monochromator (with a spectral resolution of 2 nm) equipped with an electromechanical drive. Photoluminescence spectra were recorded with a cooled photomultiplier FEU-62 (with S-1 spectral characteristic). The spectral sensitivity has been calibrated against the emission of a tungsten strip lamp SI 10–300. All spectra were corrected with an allowance for the above calibration and then normalized to the integrated intensity at $T = 10$ K. The temperature of the sample, which was placed in a cryostat in the atmosphere of exchange helium gas at reduced pressure, was stabilized to within 0.5 K. For a more accurate determination of the spectral position of separate features, we made use of the R emission lines (1.788 eV) of the Cr^{3+} ion in Al_2O_3 as reference. One-photon excitation of fullerite luminescence was effected with a helium–neon laser ($E_{\text{ex}} = 1.96$ eV) at an emission power of 20 mW. In order

to remove spurious emission at plasma frequencies and spurious generation lines, which could appear in the spectra during recording, we used a two-prism monochromator. To avoid undesirable effects related with photo-stimulated polymerization and other photo-stimulated consequences in the samples under study, the output power of the laser was attenuated to an acceptable level with a polarizer. All luminescence studies were carried out with a laser output density not in access of 1.5 mW/mm^2. Because of that the photoluminescence spectra did not change during measurements and were well reproducible between consequent recordings for the same saturation conditions. A special honeycomb sample holder ensured efficient heat removal. Local overheating during photo-excitation did not exceed 1 K, as monitored by the behavior of the temperature dependent spectral lines associated with shallow traps of fullerite. To exclude undesirable consequences of thermocycling, we took for every subsequent photoluminescence experiment a new batch of C_{60} crystals from the entire bulk of the fullerite undergoing uninterrupted saturation.

The photoluminescence method with one-photon excitation by a He–Ne laser at an excitation power density of order 1.5 mW/mm^2 allows observation of changes in the spectra of the emission coming from ~ 10 μm deep subsurface layers of C_{60}, for the extinction coefficient at 1.96 eV amounts to [29] about 10^4 cm^{-1}. We note here that the samples for the x-ray studies carried out simultaneously [30] were prepared by crushing C_{60} single crystals to a powder with an average size of below ~ 20 μm. The fact that the depth of the optically active layer in photoluminescence measurements and the powder dimensions were comparable ensured reliability of the common sample attribution for spectroscopic and x-ray findings.

For reader's convenience we recall certain results obtained during saturation and subsequent x-ray measurements [30] of C_{60}–H_2 samples. In Fig. 1 we show how the lattice parameter a of fullerite C_{60} changed with saturation time at two saturation temperatures, the saturation pressure of H_2 gas remaining constant and equal to 30 atm. By comparing the runs for saturation temperatures $T_{sat} = 150$ and 200 °C, we conclude that for the lower saturation temperature the maximum possible saturation level has not been reached while for the higher saturation temperature after 50 h hydrogen penetrated virtually to all O-voids. As the relevant analysis shows [30], when saturated at 250 °C and higher, carbon atoms of fullerite start bonding chemically with hydrogen to form compounds $C_{60}H_x$. Leaning on this finding, in all luminescence measurements we dealt only with C_{60} samples, intercalated to various saturation levels at temperatures below 250 °C.

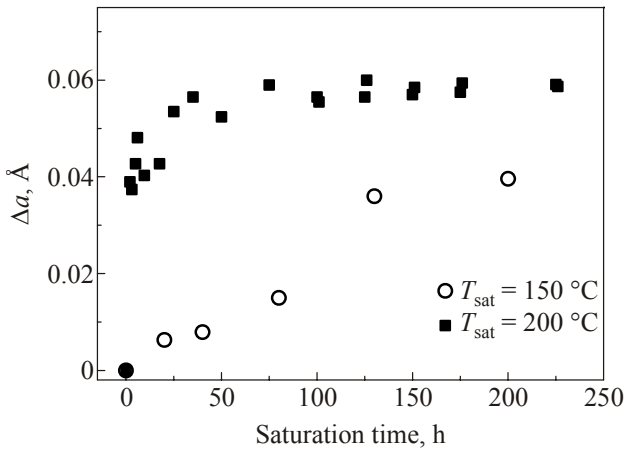

Fig. 1. Variation [30] of the lattice parameter a of fullerite C_{60} during intercalation thereof with H_2 molecules at a pressure of 30 atm and different saturation temperatures below 250 °C. The lattice parameter a was momentarily evaluated at $T = 300$ K.

3. Results and discussion

3.1. Spectral luminescence properties of pure and hydrogen-intercalated fullerite C_{60}

Photoluminescence spectra of pure C_{60} have been first measured under two-photon excitation and then correctly interpreted [22]. Since in this study the one-photon method was employed, we had to make sure that our luminescence spectra and the attribution of the bands will be in good correspondence with the above-cited results of Akimoto and Kan'no. Let us briefly recapitulate their conclusions.

The luminescence spectrum of C_{60} single crystals under two-photon excitation is a superposition of two emissions: one (A-type luminescence) is due to the recombination of Frenkel excitons localized on crystal defects, while the other (B-type luminescence) can be attributed to the recombination of singlet Frenkel excitons with participation of various intramolecular modes. A-type luminescence (its edge at 1.69 eV) can be treated as originating from inhomogeneously broadened transitions within deep X-traps, which is most likely due to a perturbed Frenkel exciton of lowered symmetry, more or less delocalized over two neighbor molecules situated close enough to a strong lattice defect. Due to the selective excitation method employed [22] it has been established that the 1.69 eV peak is the "true beginning" of the 0*–0 transition whereas the other subpeaks are vibron-assisted transitions associated with Raman-active mode of even symmetry of separate C_{60} molecules (eight h_g, two a_g, and their combinations) and accompanied by corresponding phonon wings. The above inhomogeneous broadening appears owing to orientational and translational intermolecular disorder. The B-type luminescence (beginning at 1.815 eV) looking like narrow spectral bands is associated with monomolecular singlet Frenkel exciton of the lowest possible energy. This Frenkel exciton, due most likely to Jahn–Teller-active vibrational modes, is a self-trapped small-radius polaron characterized by a small (around 5.5 meV) activation energy, which allows its migration over the crystal. Thus, given all other conditions equal, the A-type luminescence will be

also determined by the defect concentration in the vicinity of the inclusion impurity.

In the present paper we also broke the emission spectra of C_{60} obtained with one-photon excitation in features belonging to the two types of luminescence for the case of a C_{60} single crystal (dimensions 1.5×3×2 mm) with its (111) plane positioned normal to the exciting beam. In Fig. 2 we show the luminescence spectrum taken at 10 K of that C_{60} single crystal together with the constituting spectra of types A and B. The total spectrum contains narrow bands with the origin at 1.815 eV (which we ascribe to type B) as well as several broad bands of type A. After subtracting the B-type spectrum we define that the rest is mainly type A (the shaded part of the total spectrum).

In Fig. 3 we show a similar spectrum taken at 10 K of a well annealed polycrystalline sample of pure C_{60}, also broken in types A and B components. The A-type spectra of both single-crystal and polycrystal C_{60} samples were resolved into separate bands of the Gaussian shape. It should be noted here that at liquid helium temperatures the high-energy (over 1.69 eV) bands from the polycrystalline sample can be strongly suppressed, since their intensity is to a large degree due to reabsorption, because it overlaps the low-energy optical absorption spectrum of deep X-traps.

In Appendix A one can find Table 1, in which the energy positions of our spectra taken at 10 K for both pure samples are compared with similar findings of our predecessors. Taking into consideration the high degree of correspondence between our spectra and those of other authors, we came to the conclusion that all the procedures explained above can be reasonably applied in the analysis of photoluminescence of polycrystalline C_{60} samples saturated with hydrogen at a pressure of 30 atm and $T = 200$ °C during 10 saturation times of differing duration (see [30] for details). The relevant photoluminescence

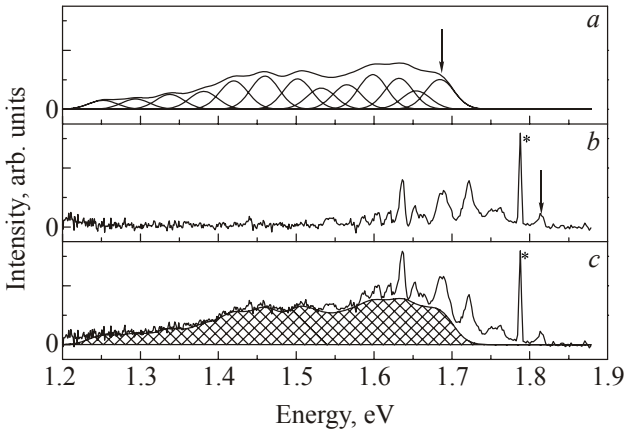

Fig. 2. The total luminescence spectrum (*c*) of a pure C_{60} single crystal at 10 K and its components A (*a*) and B (*b*). The stars denote the reference *R*-lines of Cr^{+3} in Al_2O_3. The arrows indicate exciton bands with energies 1.69 eV (*a*) and 1.815 eV (*b*). The shaded area in the total spectrum denotes the contribution due to A-type luminescence.

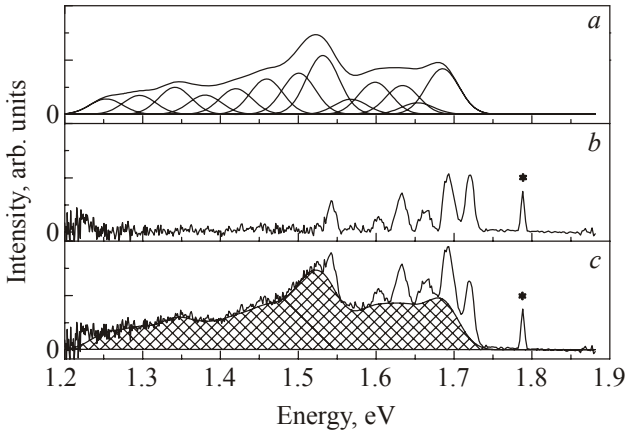

Fig. 3. Photoluminescence spectrum (*c*) of a polycrystal C_{60} samples at 10 K together with type-A (*a*) and type-B (*b*) contributions. The stars denote the reference *R*-lines of Cr^{3+} in Al_2O_3. The shaded area in the total spectrum denotes the contribution due to A-type luminescence.

spectra, all taken at $T = 10$ K, are depicted in Fig. 4 for pure C_{60} and C_{60} saturated with hydrogen to different levels. These spectra were separated in two stages, namely, 1) those with insignificant changes compared to that of pure sample (for saturation times τ shorter than 50 h);

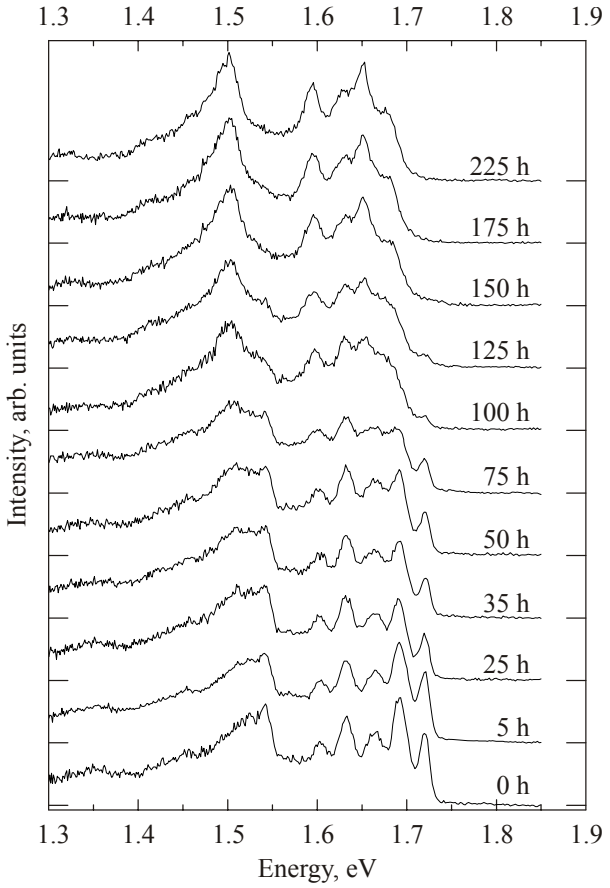

Fig. 4. Variation of the photoluminescence spectrum measured at 10 K on a polycrystalline C_{60} sample with the hydrogen saturation time. Saturation was done at a pressure of 30 atm at 200 °C.

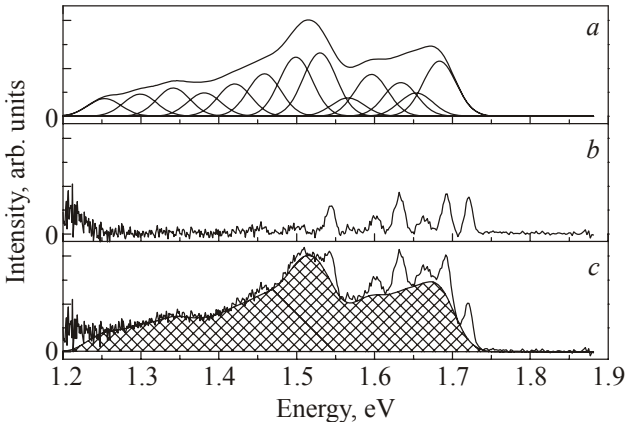

Fig. 5. The luminescence spectrum (*c*) and its type-A (*a*) and type-B (*b*) contributions from a polycrystalline C_{60} sample at 10 K. Saturation time 50 h. The shaded area in the total spectrum denotes the contribution due to A-type luminescence.

2) with pronounced changes compared to that of pure C_{60} (for τ from 75 to 225 h). These changes consisted in that, first, appreciable red shifts are clearly detectable and, second, there was a redistribution of intensities between emission bands.

All the spectra of polycrystalline samples saturated with hydrogen shown above were also broken in types A and B. In addition, these A-type spectra, exactly like for pure C_{60} samples, were into separate bands. Figures 5 and 6 show the respective total and partial spectra for two saturation times, 50 and 175 h.

Summing up, our studies allowed us to establish the following: 1) the main contribution to luminescence comes from the A-type spectra; 2) for the first stage ($\tau \le 50$ h) the A-type contribution to the total emission changes little and does not suffer any shift; 3) for the second stage ($75\ \text{h} \le \tau \le 225\ \text{h}$) the A-type contribution increases in magnitude and suffers a red shift. The variation of the position of A-type spectra of polycrystalline samples with saturation time is shown in Fig. 7. The shift of the A-type spectra as a whole was defined as an averaged shift of separate spectral bands.

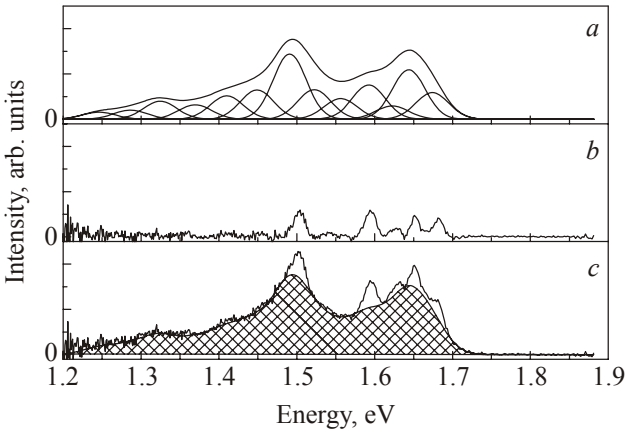

Fig. 6. The luminescence spectrum (*c*) and its type-A (*a*) and type-B (*b*) contributions from a polycrystalline C_{60} sample at 10 K. Saturation time 175 h. The shaded area in the total spectrum denotes the contribution due to A-type luminescence.

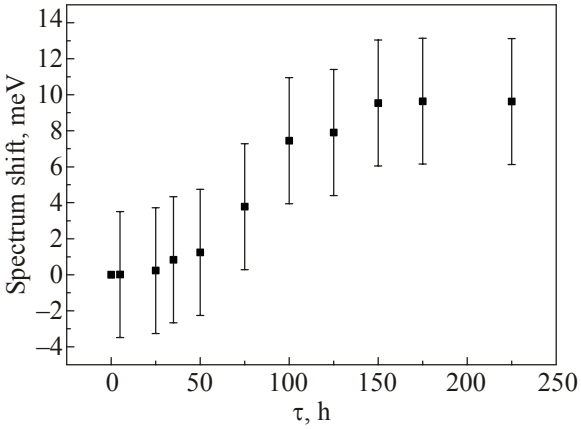

Fig. 7. The shift of A-type spectra from polycrystal C_{60} samples as a function of the hydrogen saturation time.

The shifts observed for the A-type spectra, which are related with deep X-traps, is evidence that some additional interaction between the C_{60} matrix and the H_2 impurities in octahedral voids exists. The nature of this effect is discussed in the following subsection.

3.2. Effect of hydrogen impurity molecules on the orientational glass state of C_{60}

In pure fullerite at T_c = 260 K a phase transition takes place from the high-temperature orientationally disordered phase (symmetry $Fm3m$) to the low-temperature ordered phase (symmetry $Pa3$) [4], in which the C_{60} molecules rotate in jump-like fashion. There are two different mutual orientations of every two neighboring molecules: a pentagon one, when a double bond (which is rich in negative charge) faces a pentagon (which is depleted in electrons) of the neighbor molecule, and a hexagon one when the double bond faces a hexagon. Therefore, the pentagon mutual orientation is energetically preferable. However, the energy gain between the two states is less by an order of magnitude than the energy barrier height, which controls rotation jumps of these two molecules. The relative number of pentagon/hexagon obeys the rules of thermodynamics at sufficiently high temperatures. But, as the temperature is lowered, the rotation jump frequency goes down rendering the equilibration time longer. At $T < 90$ K rotational jumps stop and the resulting state is an orientational glass with a fraction of about 18% frozen hexagon orientations [3,31]. Saturation of C_{60} with chemically neutral particles modifies its characteristics in the critical regions of the structural phase transition and of the orientational glass. In particular, T_c shifts to lower temperatures and the corresponding phase transition smoothes down [14,32–35], hysteresis appears in the temperature dependence of the lattice parameter (most expressively manifesting itself below T_c when the intercalant is xenon [36]).

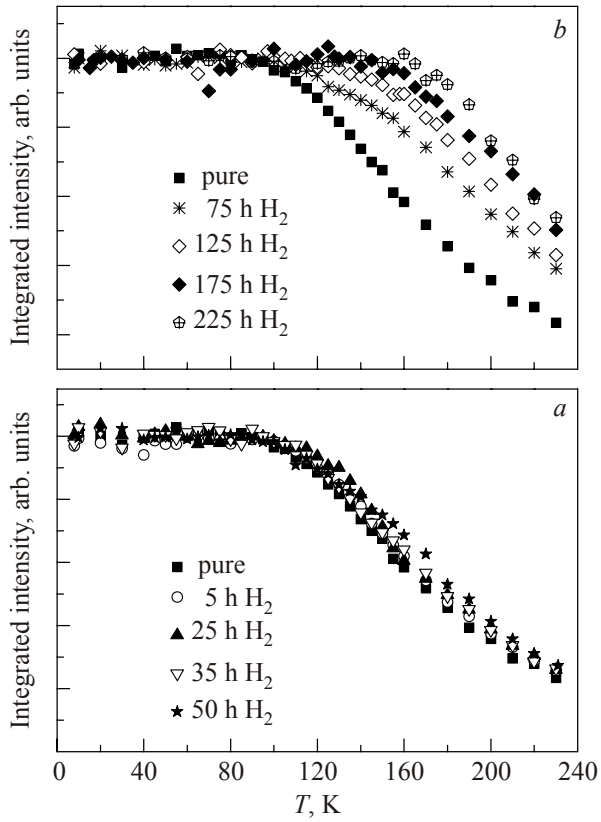

Fig. 8. Temperature dependence of the integrated intensity of the spectra normalized to the respective values at $T = 10$ K, for different saturation stages characterized by τ: "short" times $\tau = 0$–50 h (*a*); "long" times $\tau = 75$–225 h (*b*), where the $\tau = 0$ curve is shown for comparison. All curves were measured in heating regime.

Our luminescence data for doped C_{60} allow us to make reliable conclusions concerning the changes in the orientational glass formation brought about by H_2 impurities. In Fig. 8 we present the dependence of the integrated photoluminescence for two saturation stages at 200 °C. It is known [37,21] that "unfreezing" of the orientational glass in pure C_{60} entails a rather sharp decrease of the integrated intensity, which progresses as the temperature goes up. In our opinion, this effect is due not to an increasing phonon or rotation density of states [23,37] but rather to the "unfreezing" of molecular rotations.

In Fig. 8 one can see that for any regime of shorter saturation times τ (plot *a*) the $I(T)$ dependence is actually independent of τ. From this finding we infer that the orientational vitrification point stays unchanged at those saturation levels. We call attention to the fact that for $\tau \geq 50$ h (cf. Fig. 1) virtually all octahedral cavities are occupied by hydrogen molecules. At longer saturation times (cf. Fig. 8 plot *b*) the integrated intensity stays constant to appreciably higher temperatures. Treating the point, where the mechanism of emissionless deactivation changes over, as the temperature T_g, at which the orientational glass forms, we conclude that T_g varies as shown in Fig. 9.

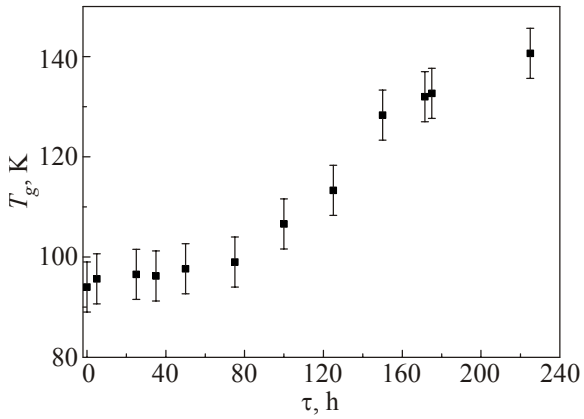

Fig. 9. Temperature dependence of the glassification point T_g of C_{60} samples on the hydrogen saturation time.

What is the cause of such behavior of $I(T)$ for $\tau > 50$ h? As established [30], after 50 h of saturation at 200 °C virtually all O-voids are filled. In principle, further saturation could promote the formation of compound $C_{60}H_x$ but in that case the increase of the lattice parameter *a* would have been essentially larger even for small *x*. Another possibility could be the process in which an O-void accommodated two hydrogen molecules. Such a possibility has been already considered [27]. If the upper curve in Fig. 1 is examined more attentively with a naked eye, one can notice that this curve has a small but positive slope for $\tau > 50$ h. There is one more [30] dependence $a(T)$ of undoubtedly physical sorption for a somewhat higher saturation temperature $T_{sat} = 230$ °C, which more clearly indicates a slowly increasing Δa upon completion of the O-void filling. The relatively small increase Δa proves that hydrogenation does not occur here. In Fig. 10 we plot estimates (for details of calculations see Appendix B) of the potential energy for one and two hydrogen molecules in an O-void. The pair of hydrogen molecules was oriented along (111) or (110) directions. Despite the fact that

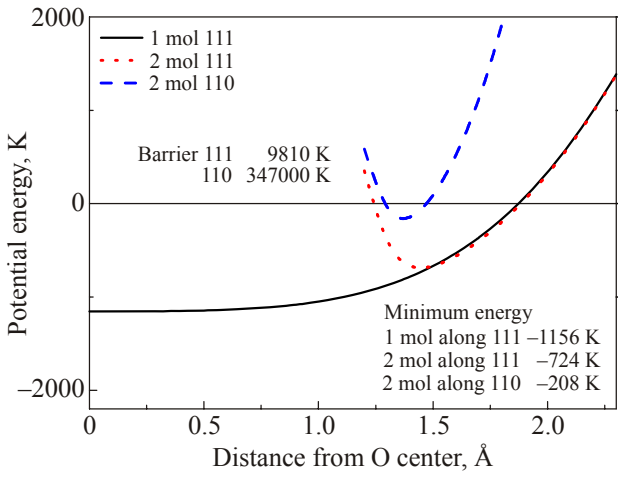

Fig. 10. The potential energies of a single H_2 molecule and a pair of molecules in the directions 111 and 110 in an octahedral cavity. The distance is measured from the void center.

a double filling is energetically unfavorable (cf. Fig. 10) the entropy contribution to the free energy at higher temperatures plays in favor of double filling [27]. Anyway, presence of two molecules must lead to stronger forces that tend to expand the octahedral cavity compared to single-molecule filling. There is a widely spread argument that expansion of O-cavities diminishes the barrier that hampers rotation. This is of course so, but only without account of the additional interaction energy between the hydrogen molecule and its nearest carbon atoms. Therefore, one can expect that, given a dopant particle inside the cavity, the counteraction to rotation (or more precisely, to rotation jumps) of C_{60} molecules will be stronger.

As shown by Akimoto and Kan'no [22], as the temperature is raised the contribution from monomeric emission drops while the emission associated with traps increases. The latter depends critically on the transport of excitons of predominantly singlet nature. The circumstance of crucial importance for this transport is the coherence of the states on the two neighbor molecules involved in the tunneling jump of the exciton. If one of the two rotates during the jump, coherence inevitably breaks down and the exciton, at least for some time, stops to progress, thereby increasing the probability of emissionless deactivation. Hence, taking into account the above arguments, we feel that the main reason behind the emission quenching in C_{60} both pure and doped (but with only one molecule in O-cavities), is the breaking of coherence of tunnelling exciton transport to traps rather than simply presence of (additional) rotational states [37], which at a temperature around 100 K cannot be plentiful. From this statement follows that the beginning of the integrated intensity drop in C_{60} is associated with the unfreezing of rotational jumps (i.e., the orientational vitrification temperature T_g), which depends on the level and nature of entities physisorbed into voids.

4. Conclusions

Over a temperature range from 10 to 230 K, photoluminescence spectra have been measured in fullerite C_{60} saturated with hydrogen at a pressure of 30 atm at different saturation temperatures from 150 to 230 °C during times τ of different duration. Following the method of Akimoto and Kan'no [22], all spectra were represented as a sum of two contributions of different origin. Making use of the analysis of saturation kinetics at different saturation temperatures [30], we dealt only with C_{60} samples saturated with H_2 in the physisorption regime.

The integrated photoluminescence intensity I in doped samples was found to be independent of the saturation time τ in samples saturated with H_2 at 200 °C during $\tau \le 50$ h for the entire temperature range of luminescence measurements. However, for $\tau > 50$ h we observed essential changes in the $I(T)$ dependence, which consisted in that I remained constant with increasing saturation time up to higher temperatures as compared to pure C_{60}.

The entire set of the above findings and a more accurate analysis of the dependence of the lattice constant on τ for the saturation temperatures 200 and 230 °C allowed us to formulate the assumption that in samples prepared with $\tau > 50$ h octahedral voids begin to accommodate two H_2 molecules. This assumption is validated by the fact that the lattice parameter increase Δa for the complete double filling is appreciably larger than for the single filling but substantially smaller than that found in the regime of chemical sorption with formation of the compound $C_{60}H_x$.

Analysis of all observations relevant for the problem enabled us to conclude that the main mechanism behind the drop of the integrated luminescence intensity above T_g is the break of coherence (caused by rotational jumps of C_{60} molecules) of exciton transport to traps, which makes excitons stop thereby increasing the probability of emissionless quenching. Proceeding from this concept and other above-stated considerations, we conclude that the T_g point (above which rotational jumps occur more often with increasing temperature) increases with increasing concentration of cavities filled with two hydrogen molecules.

Appendix A. Band attribution

In Table 1 we present our data concerning the A-type peaks for single-crystal and polycrystal samples of pure C_{60} in comparison with data of other authors [22,29,38].

Table 1. Energy positions of the A-type photoluminescence band in C_{60} crystals: our 10 K data; 5 K data [22,29]; 1.2 K data [38]. The interpretation as per [22]. psb means "phonon wing"

Energy, eV; our data		Energy, eV
single crystal	polycrystal	
1.684	1.685	1.68 30*–0 [22]
1.654	1.653	1.652 $h_g(1)$, psb [22]
1.632	1.634	1.634 $h_g(2)$, $a_g(1)$, $2h_g(1)$, psb, [22]
1.598	1.598	1.596 $h_g(3)$, $h_g(4)$, $h_g(1)+h_g(2)$, psb [22]
1.565	1.567	1.565 $h_g(1)+h_g(3)$, $h_g(1)+h_g(4)$, psb [22]
1.532	1.531	
1.502	1.501	1.501 $h_g(7)$, $a_g(2)$, $h_g(8)$, psb [22]
		1.501 [38]
		1.472 [29]
		1.467 [38]
1.460	1.459	1.45 [38]
		1.439 [38]
1.419	1.419	1.427 [29]
		1.406 [38]
		1.402 [29]
1.381	1.380	1.379 [29]
1.338	1.3426	1.352 [29]
		1.330 [29]
1.294	1.296	1.305 [29]

The main peaks are interpreted according to results [22], in which the corresponding investigations were carried out within the spectral range 1.9–1.45 eV. In other studies [29,38] it has been found that the lines observed within the low-energy spectral region 1.501–1.305 eV are due to the recombination of triplet excitons captured by deep traps. As one can see from this Table, there is a good (to within ± 1 nm) agreement between our data for single-crystal and polycrystal samples of pure C_{60} and the data of Akimoto and Kan'no [22]. As to the low-energy region, the band positions from our measurements differ from those observed elsewhere [29,38]. This can mean that predominant defects differ somewhat from those present in the samples of other authors [29,38].

Appendix B. Potential energy of H_2 molecules in O-void

We calculate the potential energy of a single H_2 molecule and a pair of H_2 in an octahedral cavity within the following approximations. The discreet structure of the surface of the C_{60} molecule is disregarded; instead we represent this surface as carbon matter (60 carbon atoms) uniformly distributed over the surface $4\pi r_0^2$, where $r_0 = 3.48$ Å is the radius of the C_{60} molecule, thus making the average density of carbon atoms to be $\rho = 60/4\pi r_0^2$. The interaction between a hydrogen molecule and the surface element δS of a C_{60} molecule at a distance R from the hydrogen molecule to the C_{60} molecule center is described by the Lennard-Jones function with the combination LG parameters, $\sigma = 3.179$ Å and $\varepsilon = 32.052$ K. Integration over the fullerene molecule sphere yields for the H_2–C_{60} potential

$$\Phi = \frac{12\varepsilon\sigma^{12}}{Rr_0}\left[\frac{1}{(R-r_0)^{10}} - \frac{1}{(R+r_0)^{10}}\right] - \frac{30\varepsilon\sigma^{6}}{Rr_0}\left[\frac{1}{(R-r_0)^{4}} - \frac{1}{(R+r_0)^{4}}\right], \quad (1)$$

where R is the distance between the hydrogen molecule and the center of the C_{60} molecule. The accuracy of our interaction energy estimates can be checked, for example, against the attraction part of a more accurate potential of FitzGerald *et al*. [39]: the difference at equilibrium distance amounts to about 4%. The interaction between hydrogen molecules was represented by the Lennard-Jones function with the parameters: $\sigma_H = 2.96$ Å and $\varepsilon = 36.7$ K. Summing over the six C_{60} molecules of the octahedral cage and accounting for the H_2H_2 interaction if two of them were present in the void resulted in the curves plotted in Fig. 10.

1. K.C. Chiu, J.S. Wang, Y.T. Dai, and Y.F. Chen, *Appl. Phys. Lett.* **69**, 2665 (1996).
2. M.A. Strzhemechny and E.A. Katz, *Fullerenes*, *Nanotubes*, *and Carbon Nanostructures* **12**, 281 (2004).
3. P.A. Heiney, J.E. Fischer, A.R. McGhie, W.J. Romanow, A.M. Denenstein, J.P. McCauley, Jr., A.B. Smith, III, and D.E. Cox, *Phys. Rev. Lett.* **66**, 2911 (1991).
4. W.I.F. David, R.M. Ibberson, T.J.S. Dennis, J.P. Hare, and K. Prassides, *Europhys. Lett.* **18**, 219 (1992).
5. M.S. Dresselhaus, G. Dresselhaus, and P.C. Eklund, *Science of Fullerenes and Carbon Nanotubes*, Academic Press, San Diego (1996).
6. C.P. Chen, S. Mehta, L.P. Fu, A. Petrou, F.M. Gasparini, and A. Hebard, *Phys. Rev. Lett.* **71**, 739 (1993).
7. B. Morosin, Z. Hu, J.D. Jorgensen, S. Short, and G.H. Kwei, *Phys. Rev.* **B59**, 6051 (1999).
8. G.E. Gadd, P.J. Evans, S. Kennedy, M. James, M. Elcombe, D. Cassidy, S. Moricca, J. Holmes, N. Webb, A. Dixon, and P. Prasad, *Fullerene Sci. Technol*. **7**, 1043 (1999).
9. Y. Ye, C.C. Ahn, B. Fultz, J.J. Vajo, and J.J. Zinck, *Appl. Phys. Lett.* **77**, 2171 (2000).
10. B. Renker, G. Roth, H. Schober, P. Nagel, R. Lortz, C. Meingast, D. Ernst, M.T. Fernandez-Diaz, and M. Koza, *Phys. Rev.* **B64**, 205417 (2001).
11. K.A. Yagotintsev, M.A. Strzhemechny, Yu.E. Stetsenko, I.V. Legchenkova, and A.I. Prokhvatilov, *Physica* **B381**, 224 (2006).
12. B. Sundqvist, *Fiz. Nizk. Temp.* **29**, 590 (2003) [*Low Temp. Phys*. **29**, 440 (2003)].
13. M. Gu and T.B. Tang, *J. Appl. Phys.* **93**, 2486 (2003).
14. S. van Smaalen, R. Dinnebier, I. Holleman, G. von Helden, and G. Meijer, *Phys. Rev.* **B57**, 6321 (1998).
15. I. Holleman, *Dynamics of* CO *in Solid* C_{60}, Thesis, Katholieke Universiteit, Nijmegen (1998).
16. M. Gu, T.B. Tang, and D. Feng, *Phys. Rev.* **B66**, 073404 (2002).
17. M. Gu, T.B. Tang, and D. Feng, *Phys. Lett*. **A290**, 193 (2001).
18. A.V. Dolbin, V.B. Esel'son, V.G. Gavrilko, V.G. Manzhelii, N.A. Vinnikov, G.E. Gadd, S. Moricca, D. Cassidy, and B. Sundqvist, *Fiz. Nizk. Temp.* **33**, 1401 (2007) [*Low Temp. Phys.* **33**, 1068 (2007)].
19. A.V. Dolbin, N.A. Vinnikov, V.G. Gavrilko, V.B. Esel'son, V.G. Manzhelii, G.E. Gadd, S. Moricca, D. Cassidy, and B. Sundqvist, *Fiz. Nizk. Temp.* **35**, 299 (2009) [*Low Temp. Phys.* **35**, 226 (2009)].
20. I.V. Legchenkova, A.I. Prokhvatilov, Yu.E. Stetsenko, M.A. Strzhemechny, K.A. Yagotintsev, A.A. Avdeenko, V.V. Eremenko, P.V. Zinoviev, V.N. Zoryansky, N.B. Silaeva, and R.S. Ruoff, *Fiz. Nizk. Temp.* **28**, 1320 (2002) [*Low Temp. Phys.* **28**, 942 (2002)].
21. P.V. Zinoviev, V.N. Zoryansky, and N.B. Silaeva, *Fiz. Nizk. Temp*. **34**, 609 (2008) [*Low Temp. Phys.* **34**, 484 (2008)].
22. I. Akimoto and K. Kan'no. *J. Phys. Soc. Jpn.* **71**, 630 (2002).
23. V. Capozzi, M. Santoro, G. Perna, G. Celentano, A. Minafra, and G. Casamassima, *Eur. Phys. J. Appl. Phys.* **14**, 3 (2001).
24. S. Kazaoui, N. Minami, Y. Tanabe, H.J. Byrne, A. Eilmes, and P. Petelenz, *Phys. Rev.* **B58**, 7689 (1998).

25. W. Guss, J. Feldmann, E.O. Göbel, C. Taliani, H. Mohn, W. Müller, P. Haussler, and H.-U. ter Meer, *Phys. Rev. Lett.* **72**, 2644 (1994).
26. A.A. Avdeenko, V.V. Eremenko, P.V. Zinoviev, N.B. Silaeva, Yu.A. Tiunov, N.I. Gorbenko, A.T. Pugachev, and N.P. Churakova, *Fiz. Nizk. Temp.* **25**, 49 (1999) [*Low Temp. Phys.* **25**, 37 (1999)].
27. B.P. Uberuaga, A.F. Voter, K.K. Sieber, and D.S. Sholl, *Phys. Rev. Lett*. **91**, 105901 (2003).
28. S.A. FitzGerald, R. Hannachi, D. Sethna, M. Rinkoski, K.K. Sieber, and D.S. Sholl, *Phys. Rev.* **B71**, 045415 (2005).
29. V.V. Kveder, V.D. Negrin, E.A. Shteinman, A.N. Izotov, Yu.A. Osipyan, and R.K. Nikolayev, *Zh. Eksp. Teor. Fiz.* **113**, 734 (1998).
30. K.A. Yagotintsev, I.V. Legchenkova, Yu.E. Stetsenko, P.V. Zinoviev, V.N. Zoryanski, A.I. Prokhvatilov, and M.A. Strzhemechny, to appear in October issue of *Fiz. Nizk. Temp.* **38** (2012).
31. W.I.F. David, R.M. Ibberson, and T. Matsuo, *Proc. R. Soc.* **A442**, 129 (1993).
32. G.H. Kwei, F. Trouw, B. Morosin, and H.F. King, *J. Chem. Phys*. **113**, 320 (2000).
33. K.A. Yagotintsev, Yu.E. Stetsenko, I.V. Legchenkova, A.I. Prokhvatilov, M.A. Strzhemechny, E. Schafler, and M. Zehetbauer, *Fiz. Nizk. Temp.* **35**, 315 (2009) [*Low Temp. Phys.* **35**, 238 (2009)].
34. B. Morosin, R.A. Assink, R.G. Dunn, T.M. Massis, and J.E. Scherber, *Phys. Rev.* **B56**, 13611 (1997).
35. T.B. Tang and M. Gu, *Fiz. Tverd. Tela* **44**, 607 (2002).
36. A.I. Prokhvatilov, N.N. Galtsov, I.V. Legchenkova, M.A. Strzhemechny, D. Cassidy, G.E. Gadd, S. Moricca, B. Sundqvist, and N.A. Aksenova, *Fiz. Nizk. Temp.* **31**, 585 (2005) [*Low Temp. Phys.* **35**, 445 (2005)].
37. E. Shin, M. Lee, D. Kim, Y.D. Suh, S.I. Yang, S.M. Vin, and S.K. Kim, *Chem. Phys. Lett.* **209**, 427 (1993).
38. D.J. van den Heuvel, I.Y. Chan, E.J.J. Groenen, J. Schmidt, and G. Meijer, *Chem. Phys. Lett.* **231**, 111 (1994).
39. S.A. FitzGerald, T. Yildirim, L.J. Cantadonato, D.A. Neumann, J.R.D. Copley, J.J. Rush, and F. Trouw, *Phys. Rev.* **B60**, 6439 (1999).